# Pre-processing of hyperspectral images. Essential steps before image analysis

2 authors:

Maider Vidal
Universidad del País Vasco / Euskal Herriko Unibertsitatea
20 PUBLICATIONS   568 CITATIONS

SEE PROFILE

José Manuel Amigo
Universidad del País Vasco / Euskal Herriko Unibertsitatea
181 PUBLICATIONS   4,215 CITATIONS

SEE PROFILE

Some of the authors of this publication are also working on these related projects:

Investigation on milk foam quality for use in espresso based milk drinks View project

Agricultura Inteligente - Sensores ópticos de espectroscopia del infrarrojo cercano (NIR) e imagen hiperespectral combinados con inteligencia artificial para el control de la calidad interna de agroberries View project
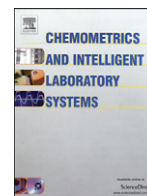
# Pre-processing of hyperspectral images. Essential steps before image analysis

Maider Vidal [a,b,c], José Manuel Amigo [c,*]

[a] Dpto. Química Aplicada, Facultad de Química, Universidad del País vasco, 20018, San Sebastián, Spain
[b] IKERBASQUE, Basque Foundation for Science, 48011, Bilbao, Spain
[c] Department of Food Sciences, Quality and Technology, Faculty of LIFE sciences, University of Copenhagen, Rolighedsvej 30, DK-1958 Frederiksberg C, Denmark

## ARTICLE INFO

## ABSTRACT

Hyperspectral Imaging is an essential technique to deep explore surfaces in which more detail than the one provided by the single point spectroscopy is needed. Many devices for acquiring hyperspectral images have been manufactured and there is an increasing interest for improving the data analysis techniques applied to such complex datasets.

Regardless the instrumentation, the acquisition of the images is being constantly improved by setting faster and more robust detectors, including new cooling systems or improving the light sources. Nevertheless, there are several issues that must be handled before starting the data analysis of any sample (e.g. background removal, compression of the images, spiked points, dead pixels, etc.). Therefore, the step of image pre-processing is almost always required.

The aim of this paper is to show the application of some of the most common possibilities to solve the above mentioned issues before the image processing. This is done in a practical way, providing examples of their application, pros and cons as well as their implementation. For this purpose, several real examples (pharmaceutical tablets and food stuff) have been used throughout this manuscript.

## 1. Introduction

Images are versatile and useful tools to obtain both qualitative and quantitative information as they have the dual property of being large datasets and visually interpretable entities. The expansion of images as analytical tools has been carried out especially thanks to the development of imaging acquisition devices, modern computers and software, able to handle great sets of data, and data analysis methods, which allow extracting the relevant information from the images [1,2]. Thanks to this development many different disciplines have profited from image analysis, like food science [3,4], pharmaceutics [5–8], medicine [9] or quality control [10,11].

A hyperspectral image is a wide collection of data, stored in pixels, each of them usually highly correlated to their neighbors. Therefore, they are composed by thousands or, sometimes, millions of data points. Handling this amount of information and extracting the relevant information have been possible thanks to the adaptation of the classical multivariate data analysis techniques (such as Principal Component Analysis or Multivariate Curve Resolution) to the analysis of hyperspectral data cubes, showing a high utility and success in extracting the desired information [5,8].

Nevertheless, there is an important issue that sometimes does not have the deserved attention when dealing with data analysis. The presence of erroneous data values (known as dead/bad pixels are being often either zero or maximum signal value) and/or non-informative background or outliers (observations which appear to be inconsistent with the whole dataset) complicates further tasks of identification, classification or even quantification. These anomalous observations can be generated by several sources:

1) The instrument: Most of the measuring systems are based on diode array detectors or tunable filters [8]. The dysfunction, for instance, of one of the diodes in the detector array may generate dead pixels (missing or zero values), unexpected spectral readings (extreme values) [12] or spiked points in one specific wavelength.
2) The geometry of the sample: The samples might have very diverse geometry. Nevertheless, the images generated have usually a square shape and compile both external background and the interesting part of the sample.
3) The radiation: It is well known that the different spectroscopic techniques are influence by different artifacts. These artifacts are inherent to the spectral technique itself and its behavior when irradiated the sample (e.g. light scattering in Near Infrared Spectroscopy — NIR); or they can be caused by the influence of the sample when irradiated (e.g. the fluorescence background in Raman spectroscopy).

A previous step of pre-processing of the images is mandatory to warranty the full and correct application of any image processing tool or multivariate data analysis routine. There are many techniques and algorithms for image pre-processing and their application and performance

* Corresponding author.
  E-mail address: jmar@life.ku.dk (J.M. Amigo).

will depend on the type of image measured, the device used and the information expected to obtain with the analysis. In general, the aim of pre-processing is to obtain uncontaminated data for further processing. Fortunately, most of the software packages provided with the hyperspectral devices include different methodologies for image pre-processing ('cleaning' step). Nevertheless, the decision of the proper pre-processing technique or finding objective criteria to solve any of the mentioned problems is not straightforward steps.

The aim of this manuscript is to offer a vast overview of the issues arising in hyperspectral imaging before further data analysis. At the same time, we will emphasize the pros and cons of the most common methodologies that can be used to solve those problems from a practitioner point of view. This paper is addressed to shed a little of light on the way and to give a concise idea of the proper steps to follow on images pre-processing before the complete analysis of the image. Real samples with different problems will be used throughout this manuscript to exemplify the use of the different methodologies proposed (see Section 3 for further information).

## 2. Image structure

As we have stated beforehand, this paper will be focused on hyperspectral images. Nevertheless, most of the pre-processing techniques shown herein can be applied to different kinds of images, regardless the technique used for measuring it. Therefore, it is extremely important the definition of the different types of images that are usually obtained in the scientific environment and, what is more important, to know their structure in order to be able to apply the proper pre-processing technique.

Images can be classified accordingly to different properties (functionality, camera used for collecting them, type of spectroscopic radiation, etc.). Probably, the most interesting classification from a data analysis perspective is attending to their spatial structure. Generally speaking, an image is a spatial representation of an object. This representation is divided into sub-units denoted as pixels. The spatial resolution of the image varies depending of the ratio image/pixel size. When talking about hyperspectral imaging, moreover, a new concept called spectral resolution appears. That is, the amount of different information channels (wavelengths) that can be obtained for each pixel. Fig. 1 and Table 1 give an overview of the types of chemical images accordingly to their spectral resolution: Single channel, color-space/digital, multi-band (also called multivariate) images and hyperspectral images.

Single channel images are, maybe, the simplest images. If there are only two possible values for each pixel (e.g. black and white) they are known as binary images. Binary images often arise in digital image processing as masks or as the result of certain operations such as segmentation or thresholding. Single channel images can also be composed of shades of gray (gray scale images) or a grading between two different colors, denoting different intensity for each pixel.

Color-space images are those in which the color of each pixel is defined by the combination of different colors in a determined space (HSV, CMYK, CIELAB, etc.). The most commonly used is the RGB space (Fig. 1). The RGB color model roughly follows the color receptors in the human eye. In this case, each pixel contains three channels of information belonging to the values of the Red, Green and Blue channels, respectively.

Multi-band images (also called multivariate images) are those that capture individual images at specific frequencies/wavelengths, frequently separated by filters, across the electromagnetic spectrum (e.g. Ultra violet–Visible, UV–vis; Mid-infrared, IR; or Raman). The main feature of these images is that they provide information in selective and discrete channels. On the other hand, hyperspectral images are based on the same concept as multi-band images. The main difference is that hyperspectral devices provide a complete (continuous) spectrum for each pixel (e.g. IR; Near Infrared, NIR; Raman or Terahertz spectroscopy) [6–8]. Usually, the hyperspectral images taken with any

vibrational spectroscopic technique are called Chemical images [6–8]. In this manuscript, for avoiding misunderstandings, hyperspectral images of any kind will be refereed with the general term of images.

## 3. Images, experimental setup and software

The images used in this paper belong to real datasets. They are representative of the common problems that must be handled before data processing. Here, the most important features about the samples and the devices used for the acquisition are presented, encouraging the reader to check the provided references for each sample.

### 3.1. Commercial ibuprofen tablet

For Sections 4 and 7 a commercial tablet of ibuprofen 200 mg. was chosen [13]. The tablet was sectioned using a cutting blade coupled to a microscope. The transverse section of the tablet was scanned with an Auto Image Microscope connected to a Fourier Transform Near Infrared (FT-NIR). The area of the image corresponds to $4.2 \times 4.2$ mm divided into $60 \times 60$ pixels of 70 μm size. The wavelength range was from 4000 to 7500 cm$^{-1}$ with a spectral resolution of 4 cm$^{-1}$. The tablet contains a sucrose coating and a wide area of background contribution that is extremely difficult for further data analysis.

### 3.2. Barley sample

For Sections 5 and 6 a single kernel of the barley (*Hordeum vulgare* L.) is used. The NIR image was acquired using a Sapphire Matrix NIR focal plane imaging system (Spectral Dimensions now Malvern Instruments Ltd., Malvern, Worcestershire, UK). The system comprised a NIR sensitive stirring-cooled InSb Focal Plane Array detector, four quartz-halogen lamps, which provided the illumination, and 2″ polarization filters. The 81920 pixels ($320 \times 256$ array) of the camera can be directed at fields of view varying from square millimeters to square inches. This image, apart for having background contribution, contains several dead pixels and spikes.

### 3.3. Pharmaceutical tablets manufactured in the laboratory

The section about spectral pre-processing (Section 9) is covered by one tablet manufactured in the laboratory. This is a five compound tablet analyzed on a NIR line mapping system (Spectrum Spotlight 350 FT-NIR Microscope, Perkin Elmer, UK) from which 16 spectra were collected in each acquisition from a linear MCT detector array. More information about this sample can be found in [8,14–16].

### 3.4. Software

Nowadays, most of the software packages implemented in the hyperspectral devices have routines for image pre-processing. These packages may differ in the implementation of the methods and also in the possibilities that they offer. Therefore, in this paper we have used mostly in-house routines built in MATLAB (The Mathworks Inc., Natick, USA). These routines are freely available upon request (jmar@life.ku.dk). For image compression, Wavelet toolbox™ (The Mathworks Inc., Natick, USA) working under MATLAB environment has been used.

## 4. Size of the images. Image compression

Hyperspectral images are usually composed of thousands or even millions of data (e.g. one hyperspectral image of $256 \times 256$ pixels operating at 150 wavebands contains more than 9 millions of data points). This amount of information requires much storage space, large transmission bandwidths and long transmission times. Therefore, the compression of the image is sometimes very advantageous to retain only the needed information. This point is being overcome by faster and
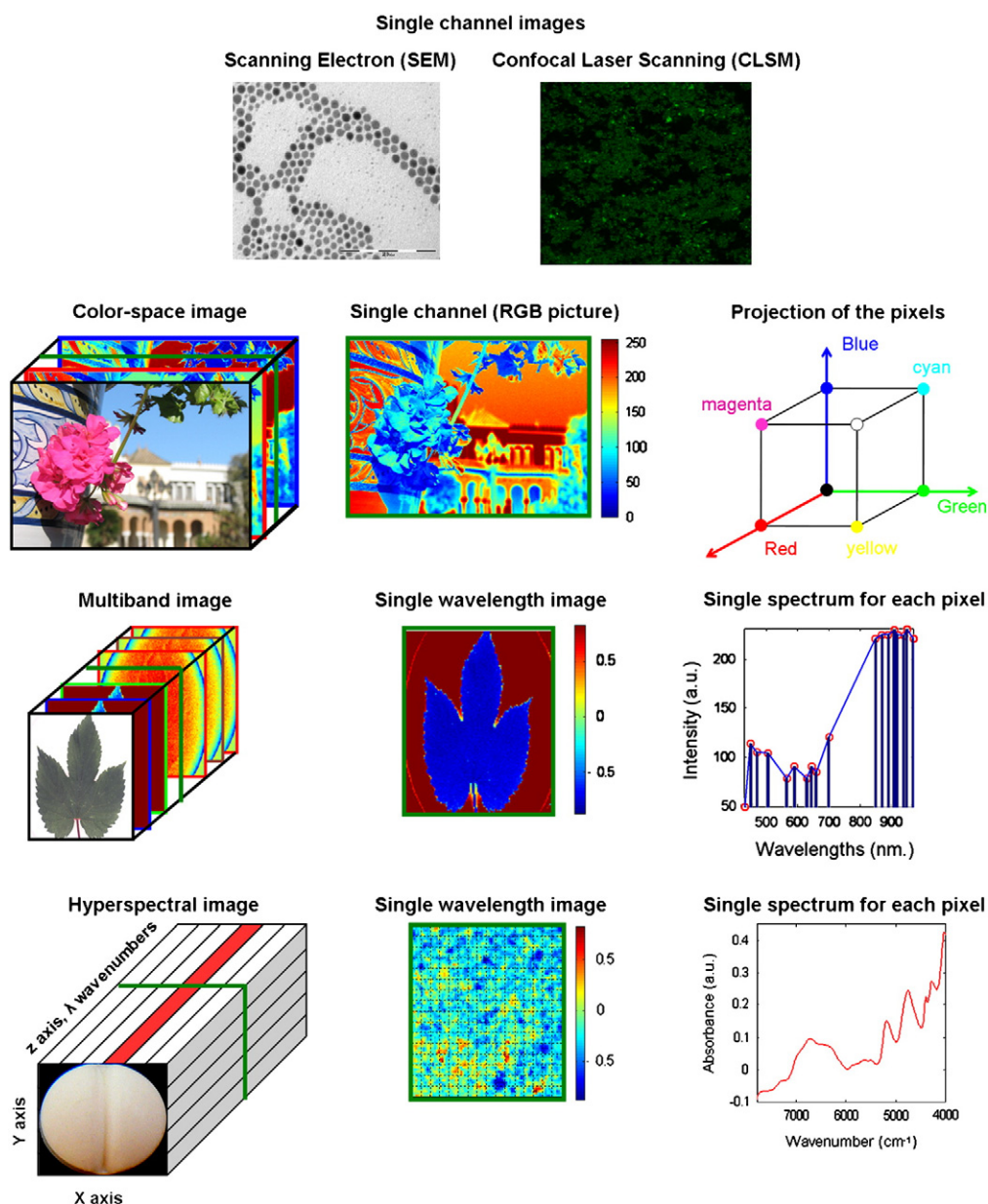
**Fig. 1.** Different types of images depending on the spectral resolution.

more powerful computers. Nevertheless, there are some situations in which storage is still an important issue (for instance, time series of images or super-resolution images).

Common ways of compressing images are bytes encoding, variable selection and data binning. Bytes encoding of the data can be applied, if possible, to reduce storage without losing information [17]. In the same way, variable selection [18] could also be an alternative to data reduction, although deciding which variables to exclude for not suffering essential losses is usually a major problem and requires previous knowledge about the data. In this sense, different mathematical strategies, like genetic algorithms [19] or interval PLS (iPLS) [20] allow variable selection in a very efficient way. Data binning has been used as a reduction technique for many years [21]. This technique can be applied in both spatial and spectral dimensions by replacing the original data values which fall in a given small interval, a bin, by a value representative of that interval.

Factor model approaches (e.g. Principal Component Analysis — PCA or Multivariate Curve Resolution — MCR) allow a drastic decrease in the dimensionality of the original image data. This is done by decomposing the unfolded three-dimensional array into a set of two sub-matrices (the score and loading matrices). The main and relevant information is preserved in the score images (containing the spatial information) and loadings (with the spectral information); while the noisy information is left out in the residuals [22]. As an example, the sample of barley used for Sections 5 and 6 has an original size of 75 MB. By keeping the first three Principal Components (PCs) of a PCA model, explaining more than 99.8% of the variance, the same analytical information can be stored into a PCA-model structure with a size of 2 MB (around 94.5% of space saved) (Table 2).

Wavelets (Wt) have widely demonstrated their usefulness as denoising, smoothing and compression tools for images [23]. In data compression, filter property of Wt allows reducing the number of elements or data with minimal loss of information [24]. Wt transforms are mainly divided into three classes: continuous, discrete and multiresolution-based wavelets. At the same time, each class contains many types of wavelets and their application will depend on the purpose and the type of the data under study.

In general, 1D wavelet transform is a well-established tool for denoising and compression of spectroscopic data. 2D wavelets, on the

**Table 1**
Examples of different types of image depending of the spectral resolution and some common applications.

| Image definitions | | | Channels | Type/example | Several applications |
|---|---|---|---|---|---|
| Digital | Single channel | Binary | 1 | Scans | Quality control [11] |
| | | Color | 1 | Photographs | Morphology/topology investigations [60,61] |
| | RGB | Color | 3 | SEM[a] | Texture/structure investigations [58,61,62] |
| | | | | TEM[b] | Cancer investigations [63] |
| | | | | AFM[c] | |
| | | | | SFM[d] | |
| | | | | Medical imaging | |
| Multivariable | Multiband | | Discrete | Vis[e] | Food/agricultural research [2,64] |
| | Hyperspectral | | Complete spectrum | NIR[f] | Pharmaceutics [5–8] |
| | | | | SWIR[g] | Geology/atmosphere [65] |
| | | | | MWIR[h] | Materials characterization [66] |
| | | | | LWIR[i] | Agriculture [67] |
| | | | | Terahertz | Environment [68] |
| | | | | Raman | |
| | | | | Fluorescence | |

[a] Scanning electron microscopy.
[b] Transmission electron microscopy.
[c] Atomic force microscopy.
[d] Scanning force microscopy.
[e] Visible.
[f] Near Infrared.
[g] Short wavelength infrared.
[h] Medium wavelength infrared.
[i] Long wavelength infrared.

other hand, have been successfully used for compressing [25] or de-noising images [26], time series of NIR spectra [27] or ion mobility spectra [28]. A common practice with multiband or hyperspectral images is the unfolding of the three-dimensional data cube of dimensions $(I, J, \lambda)$ into a two-way data set $(I^* J, \lambda)$ before applying wavelets. Nevertheless, the compression with 2D wavelets of these unfolded images can arise problems since the spatial localization of spectral information is lost. In this case, 3D wavelet transforms are advisable [29,30]. They combine the 2D wavelet transform for compressing the spatial information and the 1D wavelet transform for compressing the spectral information.

Among the most used Wt for hyperspectral image compression are the Daubechies family of orthonormal wavelets. They are discrete wavelet transforms and are named from D2 to D20. The index number refers to the number of coefficients to be calculated. Each wavelet has a number of zero moments or vanishing moments equal to the half of the number of coefficients. D2 (also called Haar wavelet) has one vanishing moment, D4 has two, etc. A vanishing moment limits the ability of the wavelet to represent polynomial behavior or information in a signal. For example, D2 with one moment easily encodes polynomials of one coefficient, or constant signal components. D4 encodes polynomials with two coefficients (constant and linear signal components); and D6 encodes 3-polynomials (constant, linear and quadratic signal components) [31]. To this point, it must be said that the final choice of the most suitable wavelets for compression will depend on the type of hyperspectral data, the level of noise and the quality of the data.

Up to now, no clear relationship between resulting compression and Wt type has been found. Vogt et al. [29] proposed the use of Haar wavelet for hyperspectral cubes if acceleration factors are of utmost importance. However, the use of D12 is advisable if retaining spatial resolution is more important than spectral information [29]. In general, a compromise between high speed computation and low resolution loss is pursued. In this sense, the same authors recommended the use of D8 wavelet. On the other hand, they discouraged to use D4 and D20 as these wavelets performed comparatively poorer than other Daubechies wavelets. Furthermore, they demonstrate that D20 is the one performing significant slower compression.

To compare the performance of different Wt (Haar-D12 – referring to the use of Haar wavelet in the both spatial dimensions and D12 in the spectral dimension — D4, D8 and D20), PCA models were calculated on the original sample of ibuprofen tablet and on the reconstructed compressed sample generated by each Wt after inverse transformation; in order to compare their performance, the loss of spatial resolution between the original image and the reconstructed one at one specific wavenumber (5748 cm$^{-1}$) was calculated as shown in Eq. (1).

$$\text{Loss of resolution} = \frac{\sum_{i=1}^{I} \sum_{j=1}^{J} \frac{P^*_{i,j}}{\left\| P^*_{i,j} \right\|}}{\sum_{i=1}^{I} \sum_{j=1}^{J} \frac{P_{i,j}}{\left\| P^*_{i,j} \right\|}} \tag{1}$$

where $P^*_{i,j}$ and $P_{i,j}$ represent each pixel of the reconstructed and original images, respectively, being $I$ and $J$ the spatial dimensions.

Fig. 2a represents the original false color image obtained at 5748 cm$^{-1}$ and the loadings of a PCA model performed on the original image. The loss of resolution image and the loadings for each Wt after the PCA models are depicted in the subsequent figures (Fig. 2b to e). It should be pointed out that the dimensions of the reconstructed images are the same as the original one. In the loss of resolution pictures, intensities close to 1 indicated high match between the original and the reconstructed image.

In general terms, the loss of resolution showed that the information retained was close to the original one (most of the intensity values in the loss of resolution images were close to 1). The loading profiles are also well retained. There are only minor changes in the shape of the
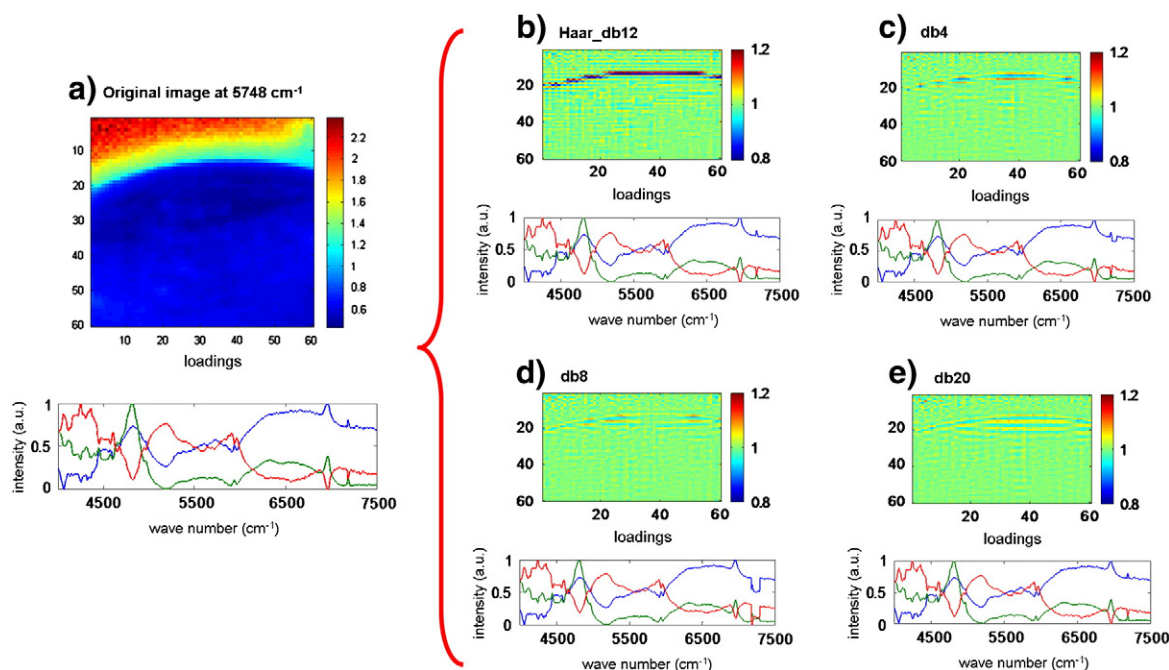
**Table 2**
Pearson correlation coefficients between the loadings of the compressed images by different wavelet selection and the original image and the percentage of compression for each wavelet and a PCA model.

| | PC1 | PC2 | PC3 | % compression |
|---|---|---|---|---|
| Haar-D12 | 0.9999 | 0.9999 | 0.9998 | 75.0 |
| D4 | 0.9994 | 0.9998 | 0.9997 | 70.3 |
| D8 | 0.9880 | 0.9992 | 0.9904 | 62.3 |
| D20 | 1.0000 | 1.0000 | 0.9999 | 32.0 |
| PCA compression | – | – | – | 94.5 |

**Fig. 2.** a) False color image of the original sample at 5748 cm$^{-1}$ and the loadings obtained by a PCA model. b, c, d, e) The loss of resolution false color images and the corresponding loading plot of the PCA models calculated on the compressed images.

loadings of the compressed images compared to the loadings obtained for the original image (e.g. the downwards peak around 7200 nm$^{-1}$ in the first component loading for the D8 compressed image), giving high values of similarity (Table 2). In this case, Haar-D12 and D20 performed slightly better than D4 and D8 in terms of loss of resolution. Considering computation time is fair to say that Haar-D12 is the wavelet combination that best overall performed in this case.

Fig. 2 also shows the appearing of a crossing line from left to right in all the compressed images. This is due to higher values of loss of resolution along this section of the tablet. This line is especially highlighted when the Haar-D12 wavelet was used for compression. In this case, it could be expected such behavior, since this area corresponds to a sharp change in the structure of the tablet (moving from the inner core of the mixture to the different layers of the coating. See [13] for further information).

Obviously, the use of any compression tool offers substantial benefits in saving storage, but also several drawbacks, like the loss of spectral and spatial resolution in the case of binning or the difficulty of choosing the number of components in the case of PCA or MCR. Another drawback is that some methods, like PCA or MCR, are highly sensitive to spikes; and, depending on the software, some of the common routines used for multivariate analysis can handle a limited amount of missing values (in the case of having dead pixels) or even none. This issue could be overcome with a previous step of spike/dead pixel detection and replacement. These issues will be introduced in Sections 6 and 7 of this manuscript.

## 5. Background removal. Regions of interest (ROI)

The geometry of the samples in the acquisition of the images plays an essential role in the selection of the regions of interest (ROI). Hyperspectral techniques usually acquire square images. If the sample does not cover all the scanned area, the area left outside the sample must be eliminated, since this area is usually composed by highly noisy spectra. The elimination of this area may seem a logical and simple task. Nevertheless, this selection is not straightforward. To illustrate this, the background removal of the barley sample has been studied and performed by using several methods (Fig. 3).

Selecting a threshold by using the scores of a previous PCA model to perform the background removal is a common practice. Fig. 3 on the left shows the score image of the first PC of the barley sample. Here we can clearly distinguish two main areas: the cyan/dark blue area, corresponding to the barley sample; and the red area, corresponding to background. The main feature of this sample is the appearing of a color gradient that evolves from orange to light green, being vanished into the cyan color. This gradient makes the selection of the proper threshold a hard job, since there is no clear cutting point in the image to separate the inner part of the barley grain from the different external layers and the background. Here, some options are given for the selection of the proper ROI from the PC1 score image:

1) Manual selection of the ROI: The performance of the manual selection of the ROI can be seen in Fig. 3, down right part, in which the green area represents the chosen area and the blue area represents the left out area. Evidently, by this procedure only the desired area will be analyzed. The main drawback of this methodology is when working with series of images, where more automatic and standard methodologies are preferred.

2) The use of histograms: Sharp changes in the histogram usually indicate different areas of the image. To increase these differences, first and second derivatives of the histograms are also used. In the barley sample, different cutting thresholds have been tested by observing the histogram or its derivative profiles (Fig. 3, top and bottom part). By previous experience, the proper cutting value in this case was around a value of the scores between 5.5 and 6. In this case, neither the histogram, nor its derivative profiles offered a clear threshold point in the score range mentioned before.

3) Manual selection of the threshold value: The manual selection of the threshold value is not exempt of problems. In our example, different cutting values offered different areas of interest, showing that, for instance, if a value of 5.2 is preferred, none of the external background is included in the model (Fig. 3). However, important information about the inner part of the sample is missed. The contrary situation is obtained if a threshold of 6 is chosen. In this case the whole sample is included as well as part of the external coatings and part of the background.
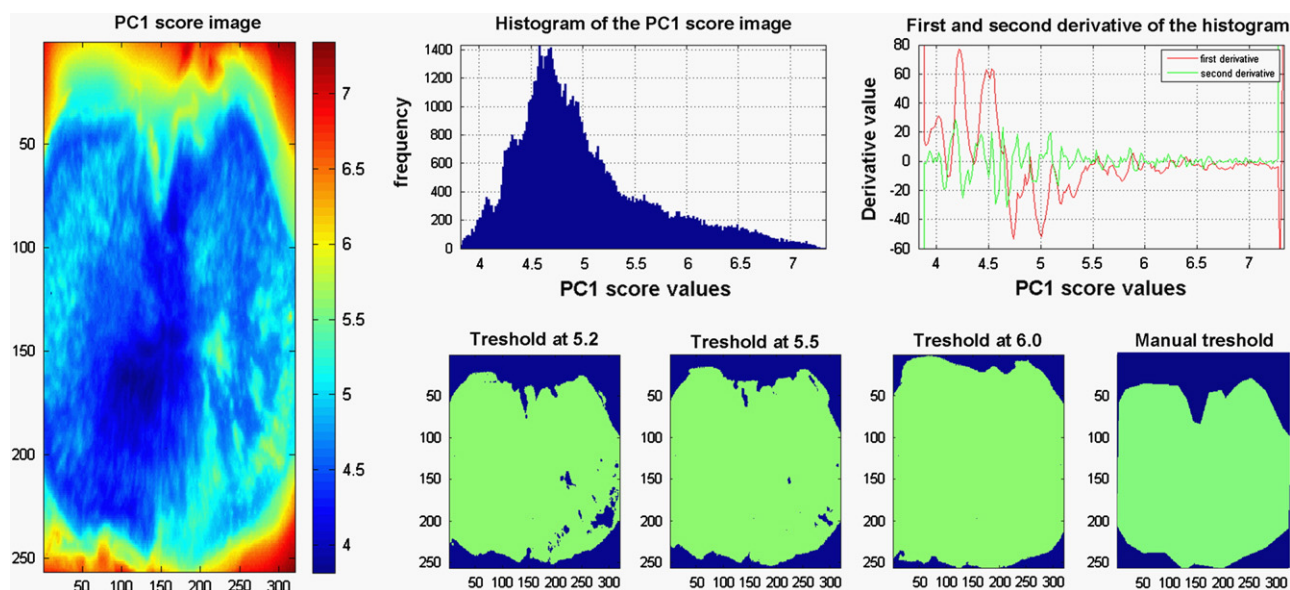
**Fig. 3.** Background removal on the barley sample (left). Top, the histogram of the false color image on the left and the derivative (first and second derivatives in red and green, respectively). Bottom, false color images obtained after applying different thresholds (the green and blue colors denote selected and unselected pixels for further analysis).

Setting a cutting threshold value is a real challenge in which, to the authors' best knowledge no objective and absolute efficient method have been reported yet. This cutting value highly depends on the type of the data and the differences between the spectral pattern of the ROI and the rest of the image.

## 6. Dead pixels

Dead pixels are usually caused by anomalies in the detectors. For instance, it is estimated that, approximately 1% of pixels when NIR detectors are used for hyperspectral imaging are considered 'dead' pixels [32]. Dead pixels may be present as missing or zero values; and their location and size may vary between being a specific pixel, a group of pixels or a complete pixel line (Fig. 4). Dead pixels can distort multivariate models; whereas many of the routines for multivariate data analysis (e.g. PCA or MCR) can handle only a limited amount of missing values. Therefore, locating and handling dead pixels is an important task for further data analysis. To illustrate this, several dead pixels have been added to the barley sample (Fig. 4).

For locating dead pixels, several criteria can be used [33], like thresholding techniques from median spectra calculated from the data [33], or more robust methods like genetic [34] or evolutionary [35] algorithms; as well as techniques such as the minimum ellipsoid (MVE) [36]. A simpler option would be the establishment of chosen criteria, considering the nature of the data. For instance, it could be considered 'dead pixel' any spectrum of the image that contains more than the 25% of zero or missing values.

Once the dead pixels have been located, one of the best choices of replacing them is the interpolation with neighbor pixels due to the evident connection in structure and correlation between neighboring pixels (Fig. 4). This interpolation is usually performed by calculating the median or the mean of neighboring values. In that sense, the use of the median might be advisable since extreme pixel values do not have so much influence as they could have in the mean calculation.
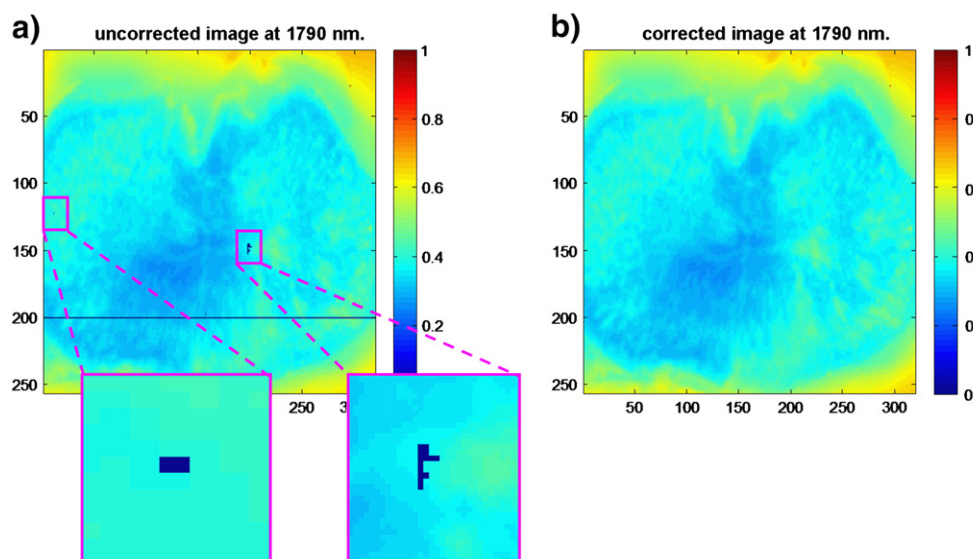


**Fig. 4.** Dead pixel interpolation in the barley sample. a) False color image at 1790 nm with different spikes. b) False color image at the same wavelength as a) but with the corrected dead pixels.

## 7. Identifying and handling spiked points

Spikes can be defined as a sudden and sharp rise followed by a sharp decline in the spectrum. They often mask details of the image and can lead to miss-identification of the signal of interest [37]. Spikes can appear due to an abnormal behavior of the detector, imperfections of electronic circuits or environmental conditions, like cosmic ray events when instruments like charge-coupled device detectors (CCDs) used for Raman imaging [38].

One of the most common spike detection methods is by manual supervision. This method, however, requires human care, it is time consuming and its performance deteriorates rapidly under low signal-to-noise ratio (SNR) [39]. In hyperspectral data, this task is even harder since there are hundreds of spectra for a data cube and not all of them contain spikes.

Recently, different techniques and algorithms have been proposed in order to remove/interpolate spikes based on the nearest neighboring pixel comparison methodology [37,40]. Beherend et al. [40] used a $3 \times 3$ window neighborhood and supposed that the probability of a spike to appear at the same wavelength CCD pixel in adjacent spectra was low. Nevertheless, although simple and easy to implement, reference spectra of low-concentration components are required. As an alternative, median and median-modified Wiener filters (MF and MMWF, respectively) have also been proposed for despiking 2D images [41]. Median filtering is similar to average filtering, in which each output pixel is set to the average of the pixel values in the neighborhood. Wiener filtering (WF), on the other hand, is a filter that tailors itself to the local image variance. It performs little smoothing where the variance is large; whereas it performs large smoothing where the variance is small. Cannistraci et al. [41] created MMWF, a nonlinear adaptive spatial filter, in order to merge the complementary qualities and abilities of MF and WF, and reciprocally, nullifying the respective defects. They demonstrate that MMWF gave the best result in minimizing spot edge aberrations while removing spike and Gaussian noise [41].

In the last times there is also an increasing interest of using Wt to detect spikes from signals [38,42,43]. For example, Ehrentreich et al. [38] proposed Daubechies, Symlet and Coiflet wavelet families as the most suitable for Raman spike de-noising. They pointed out the inefficacy of Fourier transforms in order to execute this task as Fourier analysis has the disadvantage of losing spectral information after transforming a signal into frequency domain. The proposed method is, however, not straightforward and making a distinction of spikes from chemically meaningful peaks is necessary for any of the signals to be analyzed. An appropriate selection of a threshold will be then necessary at this stage in order to make the final discrimination. Once the spike is identified, the removal is performed after projection onto the original image by interpolation or regression.

For spiking removal of a single signal, Feuerstein et al. [44] also proposed an approach based on the derivative of the signal. Spikes make the signal vary very rapidly in relation to other peaks in the signal. Their slopes are generally larger than those of the peaks of interest and when derivative is applied to the signal the large component is associated to the spike in the original data. Spikes can be separated from other forms of random noise data with the use of a histogram of the derivative signal and an appropriate threshold, removing the spikes with a linear interpolation.

A rapid and easy-to-implement methodology is necessary for the case of hyperspectral image cubes. It is clear that the threshold selection is the decisive point in order to detect and remove spikes. In general, due to the sudden and sharp rising in the signal, spikes can be easily distinguished, in most of the cases, with basic statistics. Spikes normally have a great deviation from the mean value of the spectrum. Fig. 5 shows two spectra of the commercial ibuprofen tablet with spiked points in different wavelengths. The spike in Fig. 5a appeared at the spatial location (1,5) at 7236 cm$^{-1}$; whereas the one in Fig. 5b appeared at the spatial location (16,50) at 5796 cm$^{-1}$. Considering the SNR of the image, the threshold applied for spike identification was a factor of six times the standard deviation of the mean spectrum of the image. Both spikes were detected and then substituted by interpolation with the corresponding neighbors. Therefore, a spiked point can be identified if an adequate threshold factor is implemented to the standard deviation of the mean of each spectrum. This threshold factor will depend on the experimental conditions and the type of data. Once the spikes are detected, they can be removed by substituting the spiked points by the median of the neighboring spectral channels in the spectrum so that a negligible spectrum distortion will be observed.
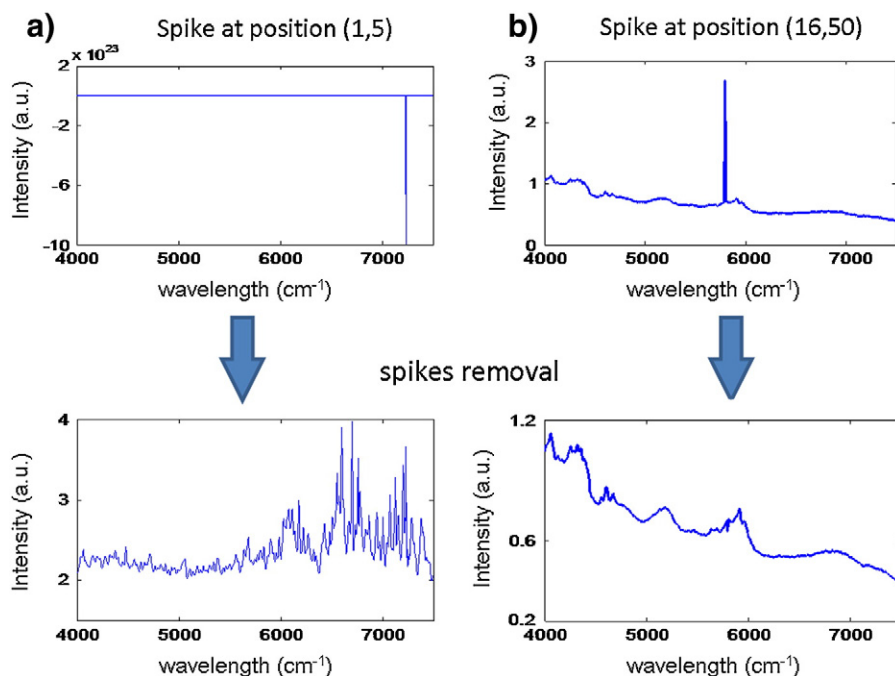


**Fig. 5.** Despiking procedure by the substitution of the spiked wavelength found at different positions of the ibuprofen commercial tablet.
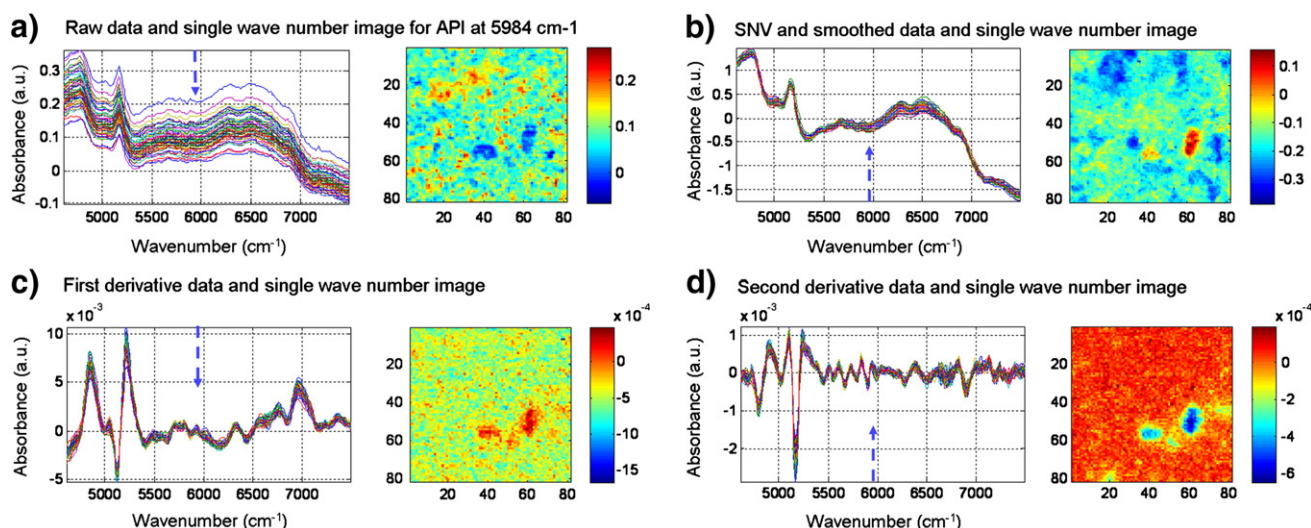
**Fig. 6.** a) NIR hyperspectral pattern obtained for one tablet containing an API and four more excipients and its corresponding chemical image at 5984 cm$^{-1}$ (further information is given in [15] and [14]. b–d) shows the application of different pre-processing methods and their chemical image at the same wavenumber. This figure is a total reproduction of Fig. 5 in [8] with permission of Springer.

## 8. The problem of outlier detection

The literature still offers no universally accepted definition of outlier [45] since rejection of outlier data is a controversial practice frowned on by many scientists and science instructors. In statistics, outliers are observations that are different from the majority of the data and determining them is most of the times a subjective exercise. While mathematical criteria provide an objective and quantitative method for anomalous data detection, they do not make the practice more scientifically or methodologically sound, especially in small sets or where a normal distribution cannot be assumed.

Most of the multivariate outlier detection methods are based on Mahalanobis distance, for example re-sampling by half-means (RHM) and smallest half volume (SHV) [46]. Other methods based on robust estimates, like the Minimum Volume Ellipsoid (MVE) [47] or Minimum Covariance Determinant (MCD) [48] have also been proposed. Despite the differences between all the existing methods, there is one feature in common: most of the detection algorithms are based on the assumption that the data are normally distributed or approximately normally distributed.

In general, existing outlier detection methods have been adapted for the use in a hyperspectral image context [49]. However, if hyperspectral data are Gaussian in nature which is still an on-going debate for the scientific community and, although there is still a need for reliable and robust multiple outlier methods when data are not normally distributed, some methods based on heavy-tailed and elliptically based distributions [50,51] have already been proposed. Smetek et al. [49] have demonstrated that assuming Gaussian distribution for detecting outliers when data have more heavy-tailed distribution perfect detection can also be obtained.

Another fact of existing outlier detection methods is that they are based in the assumption that dataset represents a sample from a single 'good' population that is contaminated by outliers from different populations. In hyperspectral image analysis, however, data actually comes from multiple populations [49]. A conventional solid pharmaceutical preparation, for example, is composed by several components: the Active Pharmaceutical Ingredient (API) and the rest of excipients. Even though the parmaceutical companies are doing a high effort to pursue the total homogeneus mixture (i.e. all the pixels have the same content of compounds), this is not always completely achieved. Thus, this surface heterogeneity can make that the histogram distribution of the components does not fulfill a Gaussian distribution. Therefore, essential information of the components under study might be

removed if an algorithm based on Gaussian or normal distribution is used to detect outliers.

## 9. Spectral pre-processing

The target of spectral pre-processing is to avoid the influence of undesirable phenomena affecting the spectral measurement, like light scattering, particle-size effects or morphological differences, such as surface roughness and detector artifacts [8]. In the field of hyperspectral imaging, the most common practice is the adaptation of the well-known pre-processing techniques of classical spectroscopy. Therefore, not much will be said herein, encouraging the readers to check the supplied references. A brief and broad overview of the main spectral pre-processing techniques, de-noising, scatter correction and derivatives must be highlighted:

– De-noising: The instrumental noise can be partly removed by using smoothing techniques. Many different algorithms are used in smoothing, but Savitzky–Golay is one of the most known for this purpose [8].
– Scatter correction: Light scattering is one of the main drawbacks when, for instance, NIR spectra are measured. In this sense, Multiplicative Scatter Correction (MSC) and Standard Normal Variate (SNV) are widely applied for scatter minimization [52,53].
– Derivatives: The Savitzky–Golay filter is also used for spectral derivative in order to reduce additive effects as spectral baseline offsets and slopes. First derivative removes an additive baseline; whereas second derivative removes a linear baseline [54]. In general, derivative transform emphasizes the spectral features of the data, but it can promote an emphasis of the level of noise. Therefore, special care must be taken in the selection of the parameters to tune the filter (derivative order, polynomial order and window size) [5,13,15,53].

As it is said in Amigo [8] proper pre-processing helps in both the reduction of spectral/spatial artifacts. As a matter of example, Fig. 6 shows how the picture of one single wavelength offers different information by using different pre-processing technique. Despite the benefits of pre-processing, it can also introduce artifacts or generate the loss of important information if the proper method is not selected or correctly applied (e.g. the improper selection of the window size when Savitzky–Golay filter is applied for both smoothing and derivatives may distort the information gathered in the spectra. Small windows will increase the noise; whereas wide windows may eliminate

**Table 3**
Summary of the main pre-processing steps, the techniques for their application and their benefits/drawbacks.

| Pre-processing step | Techniques | Types of images | Benefits | Drawbacks |
|---|---|---|---|---|
| Dead pixels | Detection | | | |
| | Median spectra/thresholding [33] | Multi-band, hyperspectral | Easy to implement and calculate | Highly dependent of the S/N ration. Risk of false positives |
| | Genetic/evolutionary algorithms [34–36] | All, but with special applicability in multi-band and hyperspectral | Robust and reliable | To find the best combination of parameters to optimize the models |
| | Chosen criteria Suppression | All | Easy to implement and calculate | Difficulties in finding the proper threshold |
| | Neighboring interpolation | All | Easy to implement and calculate | If the cluster of dead pixels is big, there could be the risk of losing resolution in this area |
| Spikes | Detection | Digital images that contain more than one spectral channel (e.g. RGB), multi-band, hyperspectral images | | |
| | Manual inspection | | Robust and reliable | Time consuming. Especially in hyperspectral images |
| | Neighboring filters [37,40,41] | | Robust and reliable | To find the best combination of parameters to optimize the filters. When the background is an important part of the image, there may be problems to differentiate the spikes |
| | Wavelets [38,42,43] | | Robust and reliable | The selection of the proper wavelet (in the spatial and the spectral channels) for each type of image |
| | Chosen criteria Suppression | | Robust and reliable | Difficulties in finding the proper threshold |
| | Neighboring interpolation [37,38,40–43] | | Easy to implement and calculate | |
| Background/ROI | PCA thresholding [33] | All | Robust selection of an specific area based of PC scores images | The selection of the proper threshold is tedious and not obvious in some situations |
| | Manual | | Selection of the desired area | Time consuming, especially working with time series images or large datasets |
| Spectral pre-processing | De-noising Savitzky–Golay smoothing [8] Scatter correction | Especially recommended for hyperspectral images (continuous spectrum). Special care must have when dealing with multi-band images. | Easy to implement | To find the best combination of parameters to optimize the filter, especially the window size |
| | MSC, SNV [52,53] | | Robust and direct suppression of baseline drifts: SNV does not change the shape of the spectra | Sometimes the suppression of artifacts is not totally achieved. MSC and derived techniques need additional information and may change the shape of the spectra |
| | Derivatives [5,13,15,53] | | Removal of different baseline artifacts. Derivatives also act as smoothing technique. | To find the best combination of parameters to optimize the filter. Especially the window size and the derivative order. |
| Compression | Bytes encoding [17] | All, always considering the software | Efficient compression | Only working for specific images types, depending on the software |
| | Spatial binning [21] | All. Special care must have when dealing with multi-band and hyperspectral images. | Easy to implement | Loss of spatial resolution |
| | Spectral binning [21] | | Easy to implement | Loss of spectral resolution |
| | Variable selection [18–20] | | Robust methods | To find the best model is tedious. Moreover, most of the times external information is required |
| | Factor models [22] | | Easy to visualize the needed information (Principal Components). Efficient compression | To select the proper number of Principal Components (Components) is not straightforward. Some PCA and MCR routines do not work with missing values or can handle a limited amount of them |
| | Wavelets [23–31,58] | | Efficient compression | The selection of the proper wavelet (in the spatial and the spectral channels) for each type of image |

small but informative peaks). Thus, it can be said that minimal and careful pre-processing is usually preferred [8].

## 10. Image processing

Once the image is clean, the step of processing the image starts. Image processing refers to the extraction of relevant information, both chemical and physical, from the pre-processed data in the form of easy-to-understand images by using advanced image processing and multivariate statistical methods. In the last times, the application of multivariate methodologies to the hyperspectral images has developed a special interest. This has been reflected in many manuscripts and reviews compiling all the possible applications of multivariate data analysis depending on the final target pursued [5–8,55].

Briefly, we can say that the most typical operations that are being carried out are: image segmentation, that consists of partitioning the digital image into multiple segments in order to simplify the image in more meaningful and simpler images to analyze [56], unsupervised pattern recognition [8], resolution [5], quantization of the conforming elements of the image by using Partial Least Squares Regression, Classical Least Squares or any other quantitative multivariate technique [16,57] or morphological studies [58,59].

## 11. Final conclusions

As we have seen throughout this paper, pre-processing of hyperspectral images is a mandatory step in almost all situations before further image processing. In Table 3 we have enhanced the most common procedures applied to the normal issues that can arise in this kind of data.

A final comment has to be done regarding the correct flow-chart of the application of the abovementioned methods. Fig. 7 shows different possibilities on this respect. It must be said that there is not a correct or logical order to perform image pre-processing. This highly depends on the difficulty of the data, the quality of the images, the availability of methods, the target of the analysis and the priority in the data acquisition.

As an example of the latter, working with time series hyperspectral images the priority is usually to have a robust compression methodology. Therefore, this would be the first step in normal conditions. Nevertheless, depending on the quality of the data (big areas of background, spiked points, dead pixels, noisy signals, etc.) the compression method chosen will not give the desirable results. As it has been said before, several multivariate routines cannot handle missing values or can handle a limited amount of them. Moreover, they are enormously affected by extreme values.

To some extent, interpolation of dead pixels can be advised to be the first steps to be done. Nevertheless, previous knowledge about the sample, the structure of the image, the conditions of the imaging devices and the quality of the data is mandatory in order to choose the correct pre-processing steps.
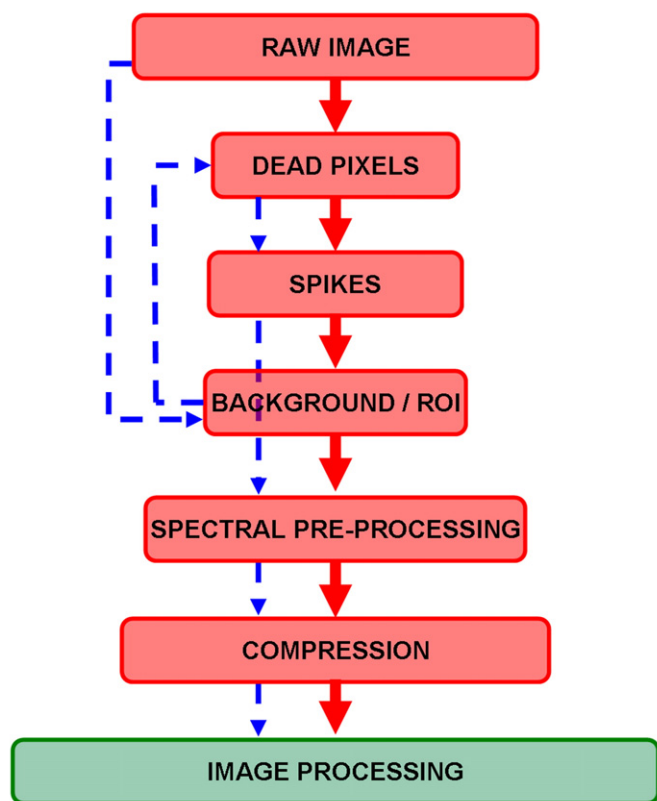


**Fig. 7.** Flow-chart of the application of different pre-processing steps. The red arrow indicates the ideal path. The blue dashed line indicates a possibility when background removal is the main critical step and is performed manually.

## References

[1] P.R. Griffiths, Imaging and Raman instrumentation for mapping and imaging, in: R. Salzer, H.W. Siesler (Eds.), Infrared and Raman Spectroscopic Imaging, Wiley VCH Verlag GmbH&Co. KGaA, Weinheim, 2011, pp. 3–62.
[2] A.A. Gowen, C.P. O'Donnell, P.J. Cullen, G. Downey, J.M. Frias, Hyperspectral imaging — an emerging process analytical tool for food quality and safety control, Trends in Food Science & Technology 18 (2007) 590–598.
[3] V. Bellon-Maurel, J. Dubois, Near-infrared hyperspectral imaging in food and agricultural sciences, in: R. Salzer, H.W. Siesler (Eds.), Infrared and Raman Spectroscopic Imaging, Wiley-VCH Verlag GmbH & Co. KGaA, Weinheim, 2009, pp. 259–294.
[4] J.C. Russ, Stereology, Image Analysis of Food Microstructure, CRC Press LLC, Boca Raton, 2005.
[5] J.M. Amigo, J. Cruz, M. Bautista, S. Maspoch, J. Coello, M. Blanco, Study of pharmaceutical samples by NIR chemical-image and multivariate analysis, TrAC-Trends in Analytical Chemistry 27 (2008) 696–713.
[6] A.A. Gowen, C.P. O'Donnell, P.J. Cullen, S.E.J. Bell, Recent applications of chemical imaging to pharmaceutical process monitoring and quality control, European Journal of Pharmaceutics and Biopharmaceutics 69 (2008) 10–22.
[7] Y. Roggo, P. Chalus, L. Maurer, C. Lema-Martinez, A. Edmond, N. Jent, A review of near infrared spectroscopy and chemometrics in pharmaceutical technologies, Journal of Pharmaceutical and Biomedical Analysis 44 (2007) 683–700.
[8] J.M. Amigo, Practical issues of hyperspectral imaging analysis of solid dosage forms, Analytical and Bioanalytical Chemistry 398 (2010) 93–109.
[9] T.W. Nattkemper, Multivariate image analysis in biomedicine, Journal of Biomedical Informatics 37 (2004) 380–391.
[10] J.M. Prats-Montalban, A. Ferrer, Integration of colour and textural information in multivariate image analysis: defect detection and classification issues, Journal of Chemometrics 21 (2007) 10–23.
[11] M. Vidal, J.M. Amigo, R. Bro, F. van den Berg, M. Ostra, C. Ubide, Image analysis for maintenance of coating quality in nickel electroplating baths — real time control, Analytica Chimica Acta 706 (2011) 1–7.
[12] J.M. Prats-Montalban, A. de Juan, A. Ferrer, Multivariate image analysis: a review with applications, Chemometrics and Intelligent Laboratory Systems 107 (2011) 1–23.
[13] C. Cairos, J.M. Amigo, R. Watt, J. Coello, S. Maspoch, Implementation of enhanced correlation maps in near infrared chemical images: application in pharmaceutical research, Talanta 79 (2009) 657–664.
[14] J.M. Amigo, C. Ravn, N.B. Gallagher, R. Bro, A comparison of a common approach to partial least squares-discriminant analysis and classical least squares in hyperspectral imaging, International Journal of Pharmaceutics 373 (2009) 179–182.
[15] J.M. Amigo, C. Ravn, Direct quantification and distribution assessment of major and minor components in pharmaceutical tablets by NIR-chemical imaging, European Journal of Pharmaceutical Sciences 37 (2009) 76–82.
[16] C. Ravn, E. Skibsted, R. Bro, Near-infrared chemical imaging (NIR-CI) on pharmaceutical solid dosage forms—comparing common calibration approaches, Journal of Pharmaceutical and Biomedical Analysis 48 (2008) 554–561.
[17] Schmalzl, Using standard image compression algorithms to store data from computacional fluid dynamics, Computer & Geosciences 29 (2003) 1021–1031.
[18] C. Abrahamsson, J. Johansson, A. Spáren, F. Lindgren, Comparison of different variable selection methods conducted on NIR transmission measurements on intact tablets, Chemometrics and Intelligent Laboratory Systems 69 (2003) 3–12.
[19] R. Leardi, Genetic algorithms in chemometrics and chemistry: a review, Journal of Chemometrics 15 (2001) 559–569.
[20] S.D. Osborne, R.B. Jordan, R. Künnemeyer, Method of wavelength selection for partial least squares, Analyst 122 (1997) 1531–1537.
[21] Y. Srinivas, D.L. Wilson, Quantitative image quality evaluation of pixel-binning in a flat-panel detector for x-ray fluoroscopy, Medical Physics 31 (2004) 131–141.
[22] A. de Juan, M. Maeder, T. Hancewicz, L. Duponchel, R. Tauler, Chemometric tools for image analysis, in: R. Salzer, H.W. Siesler (Eds.), Infrared and Raman Spectroscopic Imaging, Wiley VCH Verlag GmbH&Co. KGaA, Weinheim, 2011, pp. 65–109.
[23] R.X. Gao, R. Yan, From Fourier transform to wavelet transform: a historical perspective, Wavelets: Theory and Applications for Manufacturing, Springer, New York, 2011, pp. 17–31.
[24] P.D. Wentzell, C.D. Brown, Signal processing in analytical chemistry, in: R.A. Meyers (Ed.), Encyclopedia of Analytical Chemistry, John Wiley&Sons Ltd., Chichester, 2011, pp. 9764–9800.
[25] N. Sethi, R. Krishna, R.P. Arora, Image compression using Haar wavelet transform, Computer Engineering and Intelligent Systems 2 (2011) 1–5.
[26] Q. Lian, L. Shen, Y. Xu, L. Yang, Filters of wavelets on invariant sets for image denoising, Applicable Analysis 90 (2011) 1299–1322.
[27] J. Trygg, N. Kettaneh-Wold, L. Wallbacks, 2D wavelet analysis and compression of on-line industrial process data, Journal of Chemometrics 15 (2001) 299–319.
[28] G. Chen, P. Harrington, SIMPLISMA applied to two-dimensional wavelet compressed ion mobility spectrometry data, Analytica Chimica Acta 484 (2003) 75–91.

[29] F. Vogt, S. Banerji, K. Booksh, Utilizing three-dimensional wavelet transforms for accelerated evaluation of hyperspectral image cubes, Journal of Chemometrics 18 (2004) 350–362.

[30] J.E. Fowler, J.T. Rucker, Three-dimensional wavelet-based compression of hyperspectral imagery, in: C.-I. Chang (Ed.), Hyperspectral Data Exploitation. Theory and Applications, John Wiley & Sons, Inc., Hoboken, 2011, pp. 379–408.

[31] I. Daubechies, Ten lectures on waveletes, Ten Lectures on Waveletes, Society for Industrial and Applied Mathematics, Philadelphia, 2011, pp. 1–341.

[32] F. Firtha, A. Fekete, T. Kaszab, B. Gillay, M. Nogula-Nagy, Z. Kovacs, D.B. Kantor, Methods for improving image quality and reducing data load of NIR hyperspectral images, Sensors 8 (2008) 3287–3298.

[33] J. Burger, P. Geladi, Hyperspectral NIR image regression part 1: calibration and correction, Journal of Chemometrics 19 (2005) 355–363.

[34] P. Vankeerberghen, J. Smeyers-Verbeke, R. Leardi, C.L. Karr, D.L. Massart, Robust regression and outlier detection for non-linear models using genetic algorithms, Chemometrics and Intelligent Laboratory Systems 28 (1995) 73–87.

[35] B. Walczak, Outlier detection in multivariate calibraton, Chemometrics and Intelligent Laboratory Systems 28 (1995) 259–272.

[36] J. Cho, P.J. Gemperline, Pattern recognition analysis of near-infrared spectra by robust distance method, Journal of Chemometrics 9 (1995) 169–178.

[37] L. Zhang, M.J. Henson, A practical algorithm to remove cosmic spikes in Raman imaging data for pharmaceutical applications, Applied Spectroscopy 61 (2007) 1015–1020.

[38] F. Ehrentreich, L. Summchen, Spike removal and denoising of Raman spectra by wavelet transform methods, Analytical Chemistry 73 (2001) 4364–4373.

[39] Z. Nenadic, J.W. Burdick, Spike detection using the continuous wavelet transform, IEEE Transactions on Biomedical Engineering 52 (2005) 74–87.

[40] C.J. Behrend, C.P. Tarnowski, M.D. Morris, Identification of outliers in hyperspectral Raman image data by nearest neighbor comparison, Applied Spectroscopy 56 (2002) 1458–1461.

[41] C.V. Cannistraci, F.M. Montevecchi, M. Alessio, Median-modified Wiener filter provides efficient denoising, preserving spot edge and morphology in 2-DE image processing, Proteomics 9 (2009) 4908–4919.

[42] K. Koshino, H.Y. Zuo, N. Saito, S. Suzuki, Improved spike noise removal in the scanning laser microscopic image of diamond abrasive grain using wavelet transforms, Optics Communications 239 (2004) 67–78.

[43] P. Du, W.A. Kibbe, S.M. Lin, Improved peak detection in mass spectrum by incorporating continuous wavelet transform-based pattern matching, Bioinformatics 22 (2006) 2059–2065.

[44] D. Feuerstein, K.H. Parker, M.G. Boutelle, Practical methods for noise removal: applications to spikes, nonstationary quasi-periodic noise, and baseline drift, Analytical Chemistry 81 (2009) 4987–4994.

[45] M. Casalegno, G. Sello, E. Benfentai, Definition and detection of outliers in chemical space, Journal of Chemical Information and Modeling 48 (2008) 1592–1601.

[46] H.L. Mark, D. Tunnell, Qualitative near-infrared reflectance analysis using Mahalanobis distances, Analytical Chemistry 57 (1985) 1449–1458.

[47] P.J. Rowsseeuw, Multivariate estimation with high breakdown point, in: W. Grossmann, G. Pflug, I. Vincze, W. Wertz (Eds.), Mathematical statistics and applications, Vol. B, Reidel, Dordrecht, 1985, pp. 283–297.

[48] P.J. Rowsseeuw, K.V. Driessen, A fast algorithm for the minimum covariance determinant estimator, Technometrics 41 (1999) 212–223.

[49] T.E. Smetek, K.W. Bauer, A comparison of multivariate outlier detection methods for finding hyperspectral anomalies, Military Operations Research 13 (2008) 19.

[50] J.P. Kerekes, D. Manolakis, Improved modeling of background distributions in an end-to-end spectral imaging system model, Proceedings of the 2004 IEEE International Geoscience and Remote Science Symposium, 2, 2004, pp. 972–975.

[51] D. Malonakis, M. Rossacci, J. Cipar, R. Lockwood, T. Cooley, J. Jacobson, Statistical characterization of natural hyperspectral backgrounds using t-elliptically contoured distributions, Proceedings of SPIE 5806 (2005) 56.

[52] M. Taghizadeh, A.A. Gowen, C.P. O'Donnell, The potencial of visible-near infrared hyperspectral imaging to discriminate between casing soil, enzymatic browning and undamaged tissue on mushrooms (Agaricus bisporus) surfaces, Computers and Electronics in Agriculture 77 (2011) 74–80.

[53] Å. Rinnan, F. van den Berg, S.B. Engelsen, Review of the most common pre-processing techniques for near-infrared spectra, TrAC - Trends in Analytical Chemistry 28 (10) (2009) 1201–1222.

[54] H. Martens, T. Næs, Pretreatment and linearization, Multivariate Calibration, John Wiley&Sons Ltd., 2011, pp. 314–356.

[55] A. de Juan, R. Tauler, R. Dyson, C. Marcolli, M. Rault, M. Maeder, Spectroscopic imaging and chemometrics: a powerful combination for global and local sample analysis, TrAC-Trends in Analytical Chemistry 23 (2004) 70–79.

[56] S. Piqueras, L. Duponchel, R. Tauler, A. de Juan, Resolution and segmentation of hyperspectral biomedical images by multivariate curve resolution-alternating least squares, Analytica Chimica Acta 705 (2011) 182–192.

[57] J. Cruz, M. Bautista, J.M. Amigo, M. Blanco, Nir-chemical imaging study of acetylsalicylic acid in commercial tablets, Talanta 80 (2009) 473–478.

[58] I.C. Torres, J.M. Amigo, R. Ipsen, Using fractal image analysis to characterize microstructure of low-fat stirred yoghurt manufactured with microparticulated whey protein, Journal of Food Engineering 109 (2012) 721–729.

[59] J.C. Russ, Image Analysis of Food Microstructure, CRC Press, Boca Raton, 2005.

[60] J.R. Smith, C. Larson, S.A. Campbell, Recent applications of SEM and AFM for assessing topography of metal and related coatings — a review, Transactions of the Institute of Metal Finishing 89 (2011) 18–27.

[61] T. Miyazaki, K. Oshida, M. Endo, M.S. Dresselhaus, Application of image analysis for TEM image of acceptor graphite intercalation compound, Molecular Crystals and Liquid Crystals 340 (2000) 241–246.

[62] A. Kassner, R.E. Thornhill, Texture analysis: a review of neurologic MR imaging applications, American Journal of Neuroradiology 31 (2010) 809–816.

[63] J. de Ryk, E. Namati, J. Thiesse, G. McLennan, New imaging approaches for understanding lung cancer response to treatment, Clinical Pharmacology and Therapeutics 84 (2008) 517–522.

[64] R. Salzer, H.W. Siesler (Eds.), Infrared and Raman Spectroscopic Imaging, Wiley VCH Verlag GmbH&Co. KGaA, Weinheim, 2011.

[65] N.A. Drake, S. Mackin, J.J. Settle, Mapping vegetation, soils, and geology in semiarid shrublands using spectral matching and mixture modeling of SWIR AVIRIS imagery, Remote Sensing of Environment 68 (1999) 12–25.

[66] B. Ferguson, X.C. Zhang, Materials for terahertz science and technology, Nature Materials 1 (2002) 26–33.

[67] N.K. Noh, R. Lu, Hyperspectral laser-induced fluorescence imaging for assessing apple fruit quality, Postharvest Biology and Technology 43 (2007) 193–201.

[68] M.F. Escoriza, J.M. VanBriesen, S. Stewart, J. Maier, P.J. Treado, Raman spectroscopy and chemical imaging for quantification of filtered waterbone bacteria, Journal of Microbiological Methods 66 (2006) 63–72.